Title
Widefield multifrequency fluorescence lifetime imaging using a two-tap complementary metal-oxide semiconductor camera with lateral electric field charge modulators.

Journal
Journal of biophotonics, 12(5)

ISSN
1864-063X

Authors
Chen, Hongtao
Ma, Ning
Kagawa, Keiichiro
et al.

Publication Date
2019-05-01

DOI
10.1002/jbio.201800223

Received: 16 June 2018 | Revised: 30 October 2018 | Accepted: 9 November 2018

DOI: 10.1002/jbio.201800223

Journal of BIOPHOTONICS

FULL ARTICLE

Widefield multifrequency fluorescence lifetime imaging using a two-tap complementary metal-oxide semiconductor camera with lateral electric field charge modulators

Hongtao Chen[1] | Ning Ma[1] | Keiichiro Kagawa[2] | Shoji Kawahito[2] | Michelle Digman[1] | Enrico Gratton[1]*

[1]Laboratory for Fluorescence Dynamics, Department of Biomedical Engineering, University of California, Irvine, California

[2]Research Institute of Electronics, Shizuoka University, Hamamatsu, Shizuoka, Japan

Correspondence
Enrico Gratton, Laboratory for Fluorescence Dynamics, Department of Biomedical Engineering, University of California, 3208 Natural Sciences II, Irvine, CA 92697.
Email: egratton@uci.edu

Funding information
National Institutes of Health, Grant/Award Number: NIH P41-GM103540

Widefield frequency-domain fluorescence lifetime imaging microscopy (FD-FLIM) measures the fluorescence lifetime of entire images in a fast and efficient manner. We report a widefield FD-FLIM system based on a complementary metal-oxide semiconductor camera equipped with two-tap true correlated double sampling lock-in pixels and lateral electric field charge modulators. Owing to the fast intrinsic response and modulation of the camera, our system allows parallel multifrequency FLIM in one measurement via fast Fourier transform. We demonstrate that at a fundamental frequency of 20 MHz, 31-harmonics can be measured with 64 phase images per laser repetition period. As a proof of principle, we analyzed cells transfected with Cerulean and with a construct of Cerulean-Venus that shows Förster Resonance Energy Transfer at different modulation frequencies. We also tracked the temperature change of living cells via the fluorescence lifetime of Rhodamine B at different frequencies. These results indicate that our widefield multifrequency FD-FLIM system is a valuable tool in the biomedical field.

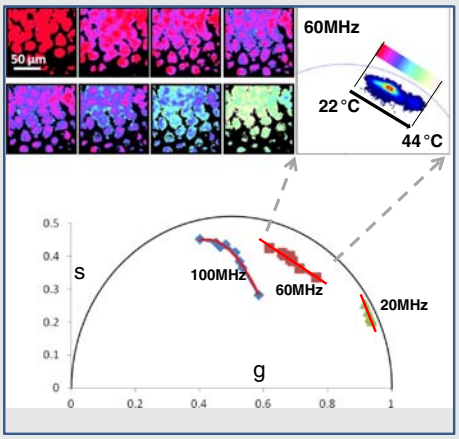

KEYWORDS
CMOS, FLIM camera, frequency-domain, harmonics, phasor plot, widefield

1 | INTRODUCTION

Fluorescence lifetime imaging microscopy (FLIM) is becoming increasingly attractive in bioimaging and potentially in medical diagnostics. It offers an imaging contrast based on fluorescence lifetime due to differences at the molecular level of microenvironments and interaction between molecules. It is an important addition and complementary to the traditional fluorescence intensity and spectrum measurements [1–3]. Most FLIM systems use laser scanning–based microscopes, that is, confocal [4, 5] and multiphoton [1, 6, 7] with single-channel detectors, such as photomultiplier tube or avalanche photodiode. Meanwhile, widefield type FLIM systems could provide higher imaging speed than scanning systems [8–10], which is particularly useful for studies with critical requirements in speed.

Frequency domain technique is commonly used in widefield FLIM experiments. It measures the fluorescence response of repetitively excited samples using high-repetition-rate lasers. The fluorescence emission at each pixel can be analyzed to determine the phase delay and the demodulation of the fluorescence emission with respect to the excitation. Using a proper sample which has a known lifetime as the reference, the fluorescence lifetime of an unknown sample at each pixel can be determined accurately and rapidly. Traditionally, such a time-resolved widefield system for frequency-domain FLIM involves an image intensifier and a camera with appropriate control, as we reported in detail earlier in [11]. In short, it requires independent control of photocathode voltage and multichannel plate voltage. To modulate the photocathode at desired frequency and phase, an extra frequency synthesizer also is needed and to be programmed or configured carefully. The resolutions (both temporal and spatial) are also limited by the image intensifier performance, for example, gating speed, defocusing effect and operation method. These difficulties can be overcome by the complementary metal-oxide semiconductor (CMOS) sensor reported here. All the frequency-domain operations are integrated into the camera firmware, and it does not have defocusing effect. Furthermore, it has a faster gating speed, and the very high harmonic content can be obtained even when a fundamental frequency of 20 MHz is used. Therefore, it is ideal for frequency-domain fluorescence lifetime imaging microscopy (FD-FLIM) measurement.

Multifrequency FLIM is useful and flexible when the sample has complex decays, for example, more than one molecular species, or when a specific modulation frequency is needed for better temporal resolution [12–14]. Using waveforms other than sine, such as square or pulse, for excitation and emission modulation allows multiple harmonic frequencies in parallel with one run of data acquisition [15–20]. Mathematically, the waveform can be decomposed into sinusoidal components by Fourier analysis, which provides separate Fourier components, that is, the fundamental frequency and harmonics. These components can be determined independently [12, 21]. At each Fourier component, multiple fluorescent molecules contribute linearly to the intensity. Thus, multiple molecular species contributing to each of these Fourier components can be extracted and displayed by the phasor approach [22]. This technique requires certain hardware support in modulation and phase control, but it results in very high time resolution based on the harmonic content over entire images.

In recent years, high frequency-modulated image sensors have been reported for FLIM. Esposito et al. reported a simple charge-coupled device (CCD)/CMOS lock-in imager for fluorescence lifetime detection [23]. This imager sensor was originally designed for 3D vision, and it was commercially available. We tested the world first commercialized FLIM CMOS camera with two taps by PCO AG (Kelheim, Germany) [24, 25]. Jan et al. and Zhao et al. developed modulated electron-multiplied (MEM)-FLIM, a CCD imager with electron-multiplication register [26, 27]. This electron multiplying CCD-based sensor can be modulated up to 80 MHz and has been used for single-image fluorescence lifetime imaging microscopy [28]. Single-photon avalanche diode arrays are also common time-resolved imagers but with less pixels [29].

Here, we report a CMOS image sensor using lateral electric field charge modulation (LEFM) and two-stage charge transfer techniques [30]. This sensor has an extremely high frequency response and low noise due to LEFM. So it is suitable for widefield multifrequency FD-FLIM. We coupled this camera to a fluorescence microscope which uses a 20 MHz supercontinuum laser as the excitation source. This picosecond laser pulse is inherently composed of a large number of harmonics at integer multiples of the pulse repetition frequency. The intrinsic response of the camera is increased by the LEFM, and the overall measured sensor response is from 180 ps (cutoff frequency ~800 MHz at −3 dB, half power point point) at 374 nm and 350 ps (cutoff frequency ~450 MHz at −3 dB, half power point point) at 851 nm [30]. These values are full width half maximum (FWHM) of the sensor responses to direct laser illumination in the time domain. Different response times are mainly due to the penetration depth and scattering of different wavelengths into the sensor region. These properties ensure that the frequency components that can be utilized are up to 400~800 MHz, depending on the wavelength. We evaluated the multifrequency components via direct measurement of the laser illumination, that is, the instrument response function (IRF) of the system. Thirty-one harmonics were obtained with 64 phase steps and 20 MHz fundamental frequency. The highest frequency is 620 MHz at the 31st harmonic component. As examples of FLIM imaging, we analyzed NIH-3T3 cells transfected with Cerulean and Cerulean-Venus constructs, respectively, for Förster resonance energy transfer (FRET) imaging at different modulation frequencies. Furthermore, the temperature measurement in live HeLa cells was performed using the fluorescence lifetime information of Rhodamine B (RhB) at multiple harmonic frequencies. Our results demonstrate that FLIM can be done in the widefield and multifrequency configuration, which can be easily combined with any widefield type fluorescence microscope, including total internal reflection fluorescence (TIRF) and single plane illumination microscope (SPIM).

2 | MATERIALS AND METHODS

2.1 | Widefield frequency-domain fluorescence lifetime microscope

One advantage of FLIM systems based on CMOS sensors is the easy configuration with existing widefield microscopes.

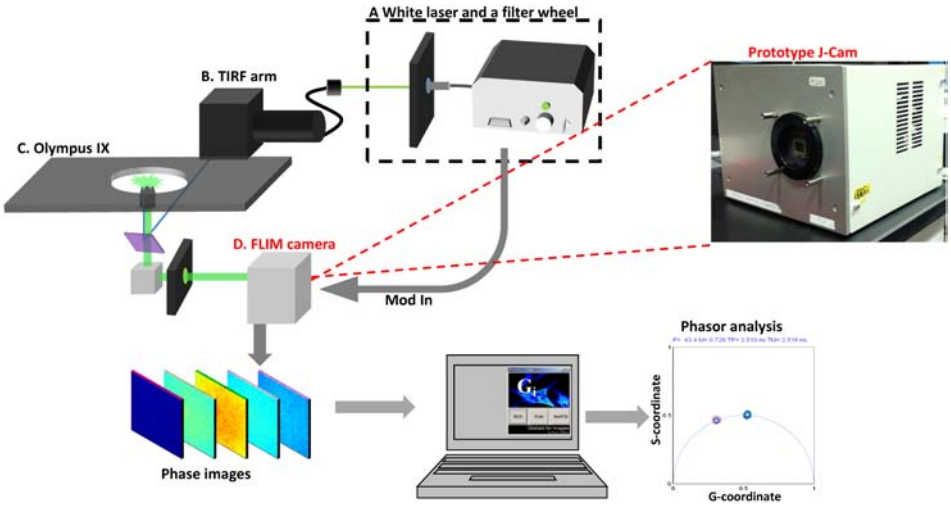

FIGURE 1 Schematic of complementary metal-oxide semiconductor (CMOS)-based widefield frequency-domain fluorescence lifetime imaging microscopy (FD-FLIM) system. A, A 10 ps, 20 MHz supercontinuum laser (SC390, Fianium Inc). Bandpass filters were used to select desired excitation wavelengths. B, the excitation beam was coupled into an Olympus TIRF microscope. C, experiments were done with a 20× (NA = 0.75) objective or a 60× (NA = 1.45) objective. D, the bottom prism reflected fluorescence signal to the FLIM CMOS camera. The FLIM camera was controlled by a computer for modulation and data acquisition

Figure 1 shows the diagram of our microscope. The FLIM CMOS camera was attached to an Olympus TIRF microscope (Olympus Americas, Center Valley, Pennsylvania). The excitation source (Figure 1A) was a 20 MHz unpolarized supercontinuum laser (SC390, Fianium Inc, Portland, Oregon). A filter-wheel with eight interference bandpass filters was used to select desired excitation wavelengths. The excitation beam was then coupled to the TIRF arm via an optical fiber (Figure 1B). After entering the microscope (Figure 1C), the beam was sent to the sample by a dichroic mirror and a 20× (numerical aperture (NA) = 0.75) objective for wide field imaging or a 60× (NA = 1.45) objective for TIRF imaging. The fluorescence signal was collected by the same objective. The bottom prism redirected the signal to the FLIM CMOS camera (Figure 1D), which was synchronized with a 20 MHz frequency output from the laser. Phase images were then acquired via the Framelink PCIe card (VCE-CLPCIe01, Imperx, Boca Raton, Florida). The camera pixel size is 11.2 μm × 5.6 μm. Sensitivity is 137ke$^-$/lux·sec. Quantum efficiency (QE) is 5%. Temporal random noise is 1.75 e$^-_{RMS}$. Time resolution is 10 ps. More specifications can be found in [30].

The number of phase images is decided according to harmonic contents and imaging speed. Harmonics are limited theoretically by the number of phase steps in each cycle (Nyquist theorem). For example, in order to get 31st (620 MHz) harmonic with 20 MHz base frequency, 64 phase images are needed during one period. The onboard field-programmable gate array (FPGA) scans 64 phases in one period and camera runs 64 exposures accordingly. Because two taps (complementary in phase) were collected simultaneously during one phase, two sets of 64 phase images were actually acquired in one scan of a fluorescence lifetime period. These two set images were than rearranged based on the phase order and averaged at each phase. The output was one set of phase images for phasor analysis. This process was used throughout this paper. All the image operations were done by the SimFCS software (www.lfd.uci.edu Irvine, California). The phasor information at different harmonic was extracted via fast Fourier transform in both phase and modulation. All data were then graphically analyzed by the phasor method, which allows fit-free fluorescence lifetime analysis.

Because FPGA performs all the necessary frequency-domain operations, for example, phase sweeping and modulation control, the complexity for the general users is greatly reduced. In a further simplified configuration, modulated laser diodes can be used as the excitation source to reduce the cost. In this case, the FPGA chip can send a desired frequency, for example, 20 MHz, to modulate the laser diode directly.

2.2 | Sample preparation

For FRET measurement in NIH-3T3 cells, two dishes of NIH-3T3 cells were transiently transfected with Cerulean and Cerulean-Venus constructs, respectively. These cells were then fixed and stored at 4°C before imaging. For FLIM measurement of RhB labeled HeLa cells at different temperatures, HeLa cells were first incubated with 10 μM RhB at 37°C and 5% CO_2 for 1 hour. Cells were then washed three times and transferred to a Tokai Hit stage incubator (5% CO_2 at room temperature) for imaging.

3 | RESULTS AND DISCUSSION

3.1 | Contributions from high-harmonic components

A picosecond excitation laser and the picosecond response of the sensor allow parallel multifrequency FD-FLIM acquisition. To validate the harmonic contents, we directly measured the 20 MHz laser illumination with 64 phase steps in

the visible (VIS) region (510/84 nm) and near-infrared (NIR) region (880/50 nm), since the camera has different cutoff frequencies in different wavelength regions, for example, 720 MHz at 472 nm and 450 MHz at 851 nm [30]. Figure 2A,B is the intensity images of the direct laser illumination with a 510/84 nm bandpass filter and an 880/50 nm bandpass filter, respectively. The speckle pattern with 880/60 nm filter was due to the fiber delivery and scattering from multiple surfaces in the optical path, which is optimized for VIS region but not for NIR region. Figure 2C shows the power spectra of 64 phase images and 31 harmonics have been plotted. This figure represents the actual frequency response of the sensor in both VIS and NIR regions. It demonstrates that the sensor has the multifrequency capability and is able to respond up to 620 MHz with 64 phase steps. However, the contribution of harmonic components in NIR region is less than it in VIS region. We also found that the odd and even numbers of harmonics show different behaviors which are likely due to the imperfection of the sensor. The phasor plots in VIS region at the fundamental frequency (20 MHz) and at the 31st harmonic (620 MHz) are shown in Figure 2D. For easy visualization, phasors are displayed at 2 ns, whereas the lifetime of the excitation laser is supposed to be 0 ns. Insets are phasor selection maps. The red regions in the inset are corresponding to the phasors inside the red circles in the phasor plots. Figure 2F is the phasor plots in NIR region at the fundamental frequency (20 MHz) and 31st harmonic (620 MHz). These results imply that our system allows FLIM measurements with multiharmonics (31 harmonics with 64 phase images) in one acquisition. It offers the capability and flexibility in using FLIM at different frequencies, for example, separating multicomponent fluorescence decays and selecting the suitable frequency for target fluorescence molecules.

In general, more phase steps sampled per period allow greater harmonic content and also result in a better discrimination of closed phasors. But, the imaging speed is slower due to the increased number of phase images. Therefore, a balance between the harmonic content and imaging speed needs to be achieved. Typical fluorescence probes ranging from 1 ns to 10 ns have the best corresponding modulation frequency from 10 to 100 MHz.

As a demonstration, we used 32 phase images (15 harmonics) per cycle to measure Rhodamine 110 solution (fluorescence lifetime 4 ns) as the reference and the Coumarin 6 solution (fluorescence lifetime 2.5 ns) as the sample. The exposure time was 100 ms, and the total imaging time was ~3.2 seconds per fluorescence lifetime image with 32 phase images. First, we calculated the power spectra of the two solutions and showed them in Figure 3A. Second, we analyzed four harmonics based on the power spectra: 20, 60 (3rd), 100 (5th) and 300 MHz (15th), whereas harmonic contents at 40, 80 MHz and so on are impaired due to

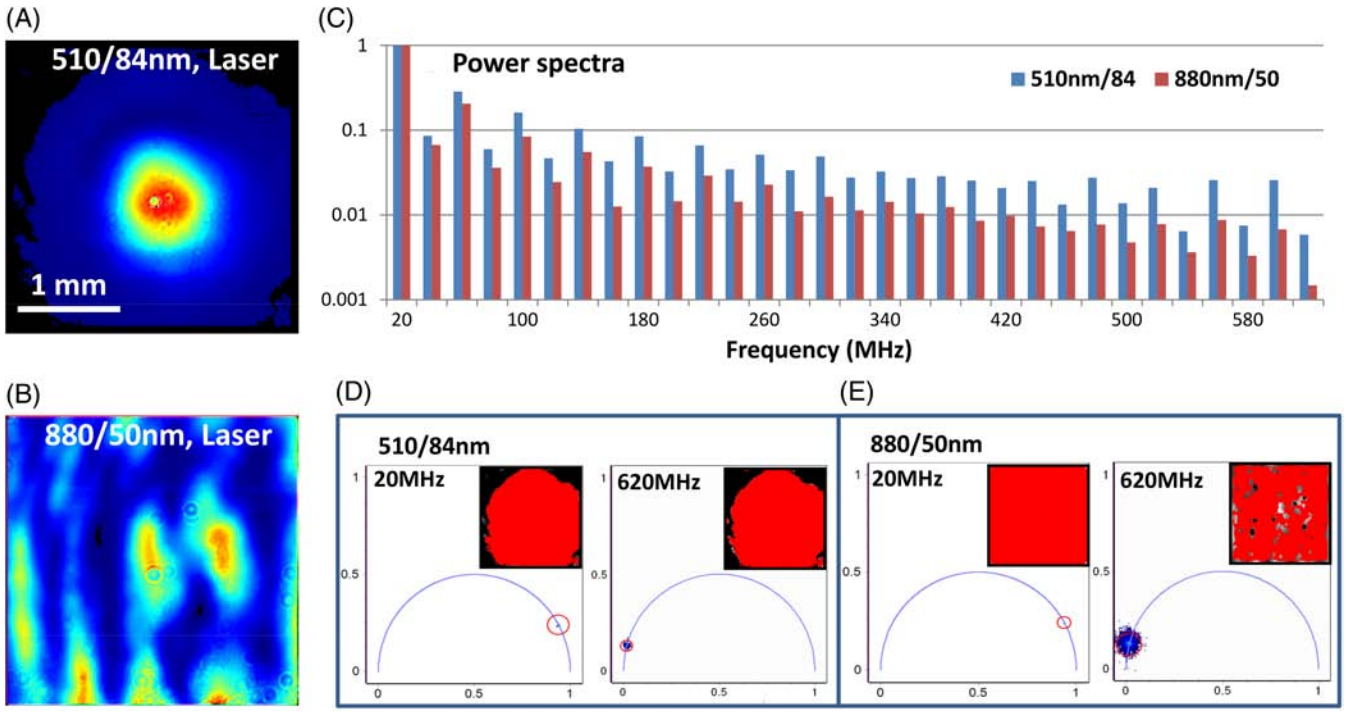

FIGURE 2 Multifrequency fluorescence lifetime imaging microscopy (FLIM) measurements a 20 MHz laser illumination with 31 harmonic contents in visible (VIS) and near-infrared (NIR) regions. The maximum frequency is 620 MHz (31st). A, laser spot in visible region (510/84 nm). B, laser illumination in NIR region (880/50 nm). C, power spectra of 64 phase images and 31 harmonics. D, The phasor plots of A at 20 and 620 MHz (the phasors are moved to 2 ns in phasor plot for easy visualization, whereas the lifetime of the excitation laser is supposed to be 0 ns). The inset is the corresponding phasor mapped image. The red region in the inset is corresponding to the phasors inside the red circle in the phasor plot. E, the phasor plot of B at 20 and 620 MHz

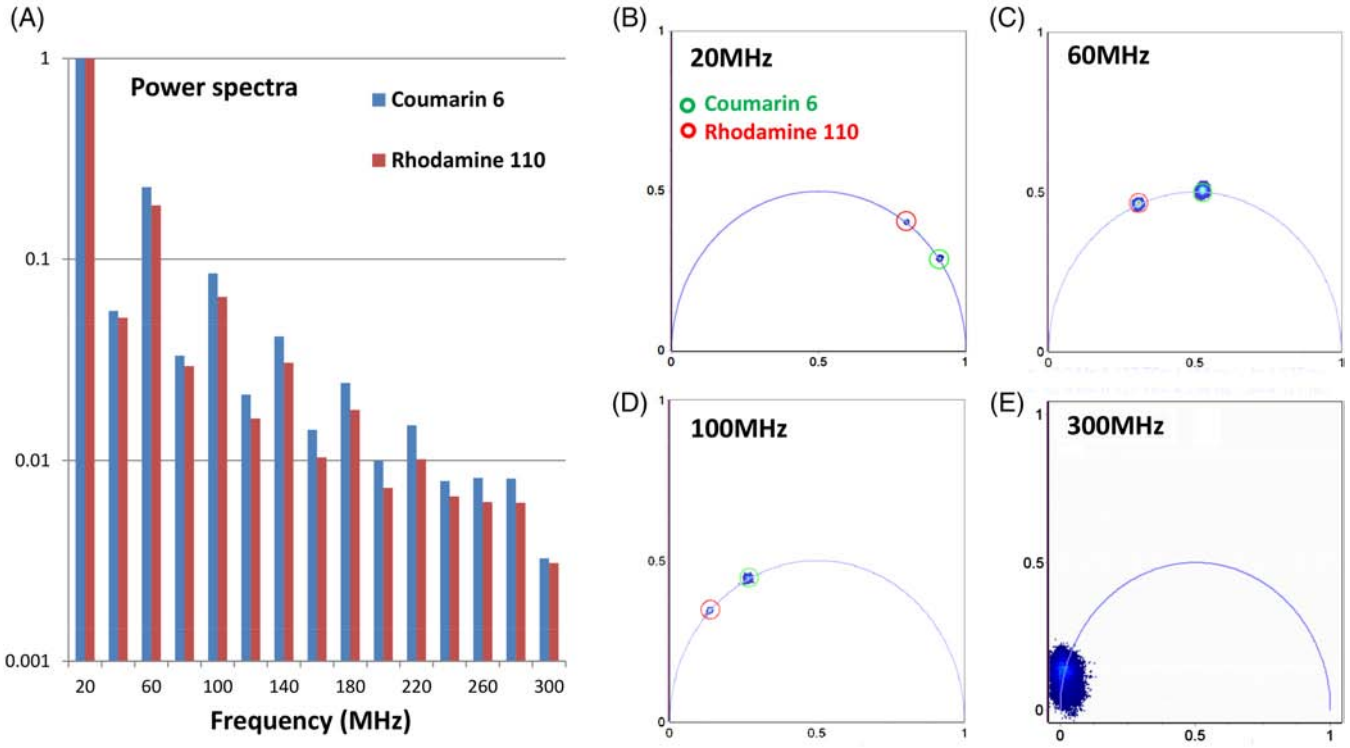

FIGURE 3 Measurement of fluorescence dyes at different harmonic frequencies with 32 phase images (100 ms exposure time). A, power spectra of Coumarin 6 and Rhodamine 110 solutions. B, phasor plot of Coumarin 6 and Rhodamine 110 at 20 MHz. C, phasor plot of Coumarin 6 and Rhodamine 110 at 60 MHz. D, phasor plot of Coumarin 6 and Rhodamine 110 at 100 MHz. E, phasor plot of Coumarin 6 and Rhodamine 110 at 300 MHz

the imperfection of the sensor. Phasors at 20 (Figure 3B), 60 (Figure 3C) and 100 MHz (Figure 3D) all show similar results. The distances between Coumarin-6 phasor spots and Rhodamine-110 phasor spots at 20, 60 and 100 MHz were calculated based on their g and s coordinates to be 0.161, 0.220 and 0.159, respectively. This result shows that 60 MHz gives the best separations of two dyes among these frequencies. However, at 300 MHz (Figure 3E), both fluorescence dyes cannot respond well, and we could not obtain valid measurements. Therefore, eight phase images (three harmonics) are sufficient for this sample and the total image acquisition can be decreased to 0.8 second.

3.2 | Measurement of FRET in NIH-3T3 cells

FRET is a mechanism due to energy transfer between two chromophores. It is extremely sensitive to small changes in distance. Measurements of FRET can be used to study the molecular interactions. Here, we measured NIH-3T3 cells transiently transfected with Cerulean (donor only, Figure 4A) and Cerulean-Venus (FRET, Figure 4B) constructs, respectively. Meanwhile, Figure 4C,D is corresponding phasor selection maps at 20 MHz. The measurement was done with 32 phase steps per cycle and the exposure time was 50 ms. The excitation filter was 438/24 nm, and the emission filter was 475/35 nm. By measuring the fluorescence lifetime change of the donor in both donor-only cells and FRET-pair cells, the FRET efficiency can be estimated.

Figure 4C shows power spectra of the donor-only cell (Cerulean) and the FRET-pair cell (Cerulean-Venus). Based on the power spectra, we extracted the phasor information at 20, 60, 100 and 140 MHz (Figure 4D-G). The FRET of SimFCS was used to estimate the FRET efficiency graphically at these frequencies in the FRET-pair cell (Figure 4B), based on the unquenched donor measured using the donor-only cell (Figure 4A). FRET efficiencies from these four phasor plots (Figure 4D-G) are independent to each other and allow the statistics of the calculation with only one measurement. Thus, the average FRET efficiency was 0.40 and the SD was 0.01.

It is interesting to investigate which frequency is best to use among available harmonics in this analysis. The separation of phasors depends on the modulation frequency and the fluorescence lifetime of sample. The distribution of phasors depends on the number of photon collected. These two facts are independent to each other. The best frequency should give the largest separation with distinguishable phasor distribution. By plotting the line profiles across the phasor distributions in Figure 4D-G, we are able to evaluate the separation of donor and FRET phasors. Figure 4H shows such profiles at 20, 60, 100 and 140 MHz. The profile at 20 MHz shows the narrowest FWHM, but the distance between two peaks is the smallest. The profile at 100 MHz has the largest distance between two peaks, but the FWHM is much broader than it at 20 and 60 MHz. The worst case is 140 MHz, which is due to the broadest FWHM and the

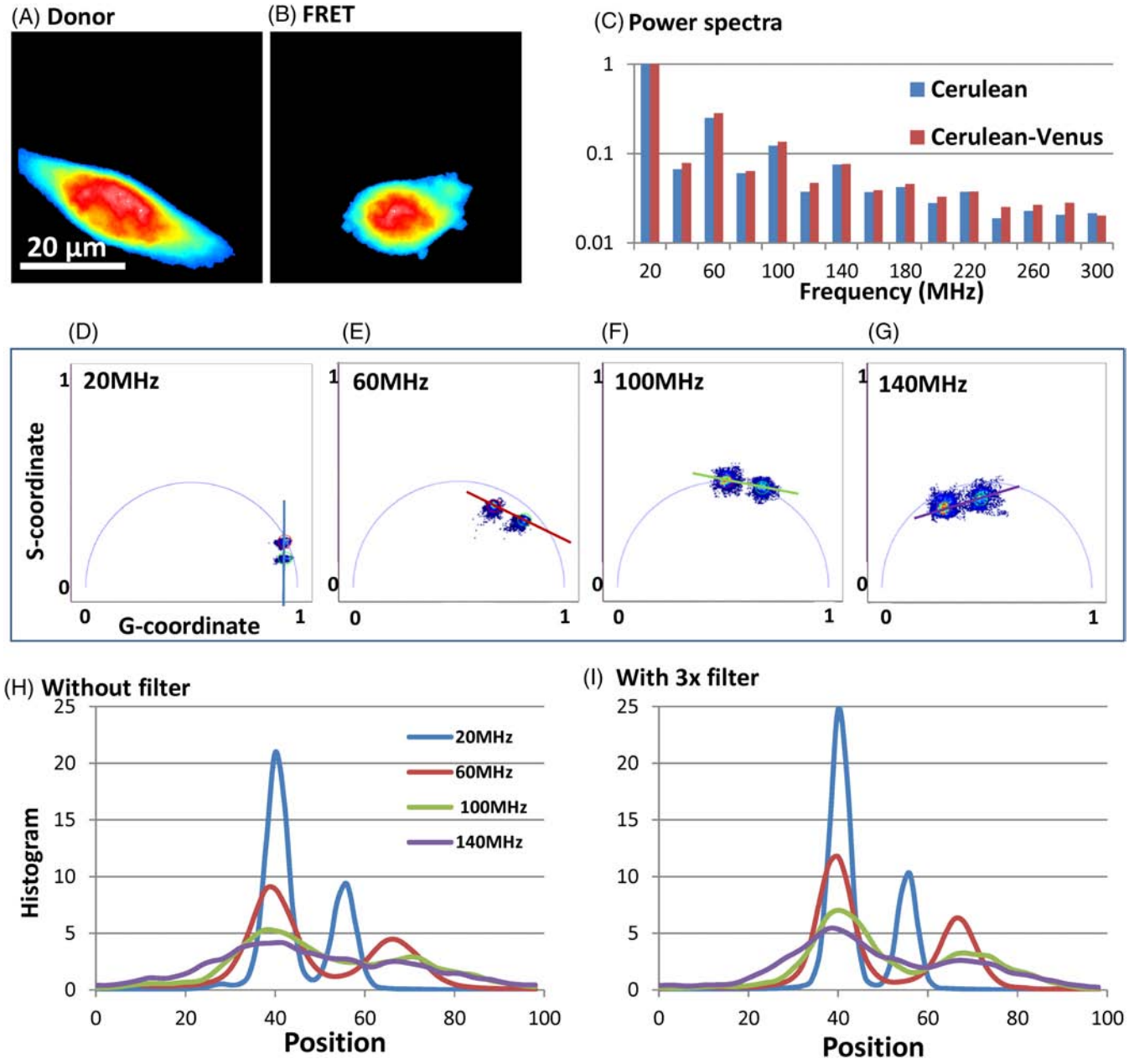

FIGURE 4 Measurement of Förster Resonance Energy Transfer (FRET) in NIH-3T3 cells. A, cell transiently transfected with Cerulean (donor) only. Scale bar = 20 μm. B, cell transiently transfected with Cerulean-Venus construct (FRET pair). C, power spectra of the cells in A and B. D to G, phasor plots at 20, 60, 100 and 140 MHz. Insets are the calculations of FRET efficiencies at corresponding frequencies. H, line profiles across phasors (in D-G) at different frequencies. I, line profiles across phasors (in D-G) at different frequencies with 3× median filter applied

distance between two peaks is smaller than at 100 MHz. Therefore, 60 MHz is a tradeoff for this measurement with certain number of photons. It offers larger separation between two peaks than at 20 MHz and more distinguishable phasor profiles when compared with 100 and 140 MHz. To narrow down the phasor distribution, the common way is to collect more photons, which will lead to longer exposure time, but hence 100 MHz can be the best frequency. The other alternate way is using the median filter which can decrease the uncertainty of the phasor location effectively [31]. With three times 3 × 3 median filter, the separation of donor and FRET is improved as shown in Figure 4I.

3.3 | Measurement of localized temperature in cells via FLIM of RhB

In biomedical research, measuring the localized temperature change within a complex biological sample is difficult but important, for example, in photothermal therapy. Various techniques have been designed to measure temperature at the microscopic scale [32]. Among them, fluorescence probes which respond to temperature changes are cheap and convenient to use. RhB is one of such sensors based either on the fluorescence intensity or the lifetime [33–35]. The fluorescence lifetime is more robust because it is not affected by the local concentration and the excitation power.

Although the fluorescence lifetime of RhB in water is well described by a monoexponential decay, the representation of such fluorescence decay in real biological samples is challenging due to the complexity at microscopic scale. Therefore, it is difficult to describe the temperature change inside biological structures via the fluorescence lifetime fitting method. Instead, the fit-free 2D graphical phasor approach is an ideal method for mapping and tracing the temperature at pixel level in biological samples.

We acquired fluorescence lifetime images of RhB-labeled HeLa cells at different temperatures varying from 22°C to 44°C. The real-time temperature was monitored by a thermometer with its probe inside the cell culture medium. The temperature control remained off until the medium temperature was at the room temperature (~22°C) and then the temperature was ramped up. The destination temperature was set to 50°C. The excitation filter was 542/27 nm, and the emission filter was 580 nm longpass. The exposure time was 100 ms, and 16 phase images were acquired. The total time for one FLIM image was ~2 seconds. We acquired FLIM data of the same field of view with a 20× objective at 22°C, 29°C, 32°C, 35°C, 37°C, 40°C, 42°C and 44°C in sequence.

Figure 5A shows the fluorescence intensity images of cells at eight different temperatures. Based on the power spectra (not shown), we extracted and analyzed the phasor information at 20, 60 and 100 MHz (Figure 5B). The center phasor plot shows the drifts of the phasor position (g and s, represents the average phasor coordinates) as a function of temperature from 22°C to 44°C at 20 (green), 60 (brown) and 100 MHz (blue). The shifts of phasors toward (1, 0) g-s coordinate demonstrate that the fluorescence lifetime of RhB in living cells becomes shorter at higher temperature. The trajectory of phasors from 22°C to 44°C at 100 MHz is the longest among all three trajectories in Figure 5B, indicating the best separation of temperatures. However, due to lower contributions of photons at this high frequency, the phasor distribution is broadened (inset 2), which lowers the temperature resolution. In contrast, the trajectory at 20 MHz is the shortest and the phasor distribution is narrowest. By displaying the g-s coordinate vs temperature, respectively, at Figure 5C, we found that (a) at 20 MHz, g was changed from 0.917 to 0.938 (1.04°C resolution) and s was changed from 0.255 to 0.203 (0.42°C resolution), (b) at 60 MHz, g was changed from 0.619 to 0.765 (0.15°C resolution) and s

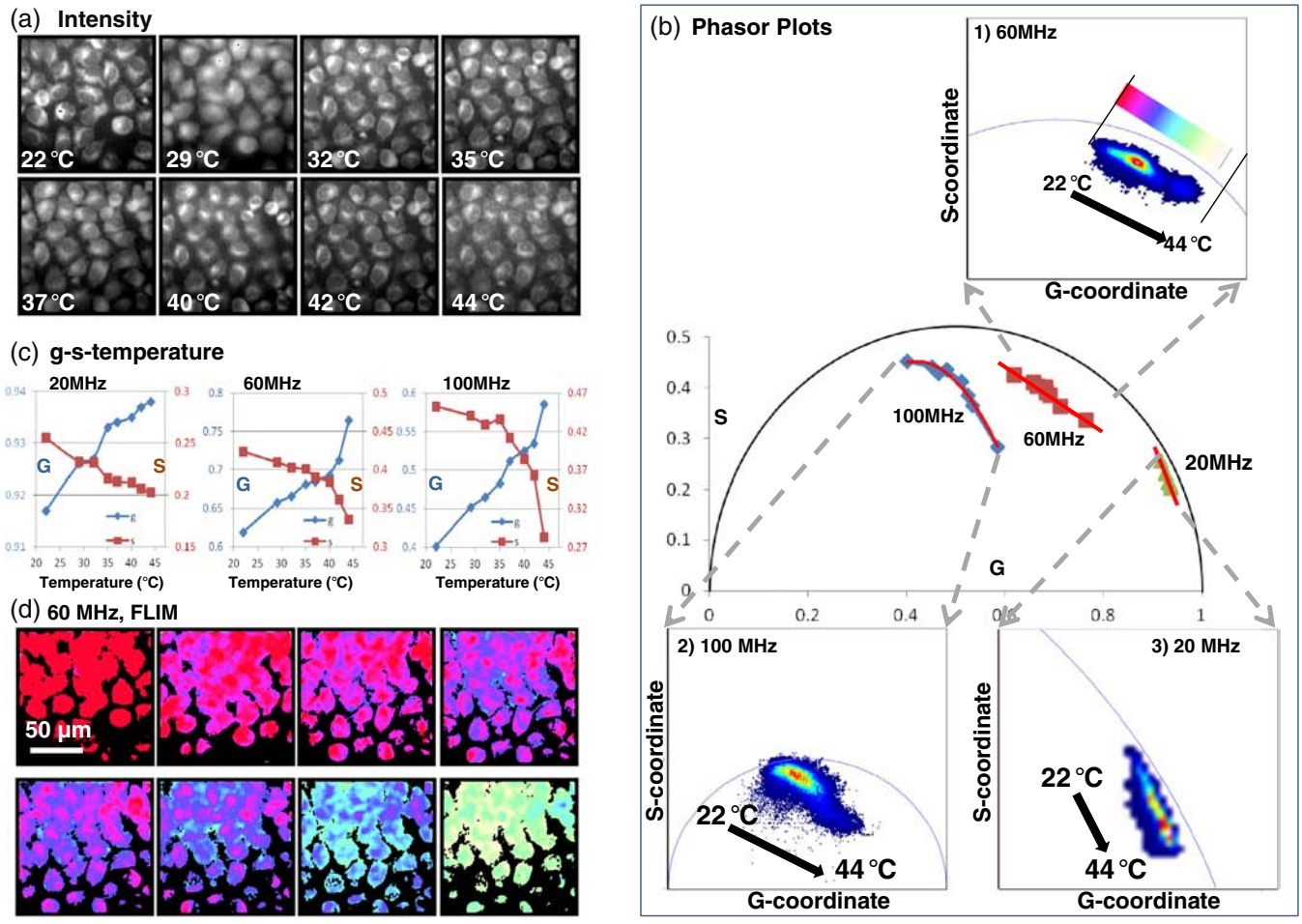

FIGURE 5 Temperature measurements in HeLa cells via fluorescence lifetime of Rhodamine B at different harmonic frequencies. A, fluorescence intensity images of same HeLa cells at eight different temperatures: 22°C, 29°C, 32°C, 35°C, 37°C, 40°C, 42°C and 44°C. B, phasor plots of fluorescence lifetime of Rhodamine B in living cells. B1-B3 show detailed phasor distributions at 60, 20 and 100 MHz with median filter applied, respectively. C, g-s coordinates vs temperature at 20, 60 and 100 MHz. D, color-coded fluorescence lifetime images of cells at 60 MHz. Scale bar = 50 µm

was changed from 0.424 to 0.336 (0.25°C resolution) and (c) at 100 MHz, g was changed from 0.401 to 0.586 (0.12°C resolution) and s was changed from 0.453 to 0.283 (0.13°C resolution). The resolution is an estimation based on the linear interpolation between points, that is, the total change of temperature divided by the total change of g or s, which can be determined with 0.001 accuracy. Phasors at 60 MHz provides similar resolutions as phasors at 100 MHz, but with a narrower phasor distribution. Therefore, we show the corresponding FLIM images at 60 MHz in Figure 5D. The color bar (Figure 5B) from red to white indicates the increase of the temperature. Interestingly, the temperature appears to be higher at cell periphery area than the middle region, which could suggest the route of heat transport. It is not caused by different intensities across cells since fluorescence lifetime is not dependent on the concentration. The first image of Figure 5A (intensity) and 5D (lifetime), which was taken at the room temperature (22°C), shows the same lifetimes with different intensities across cells. The difference of lifetime in cells only occurred when the temperature increased as shown in the rest images. Furthermore, the phasor plot also shows that there is (quasi) a linear combination of lifetimes that exclude the background or autofluorescence as a source of contamination. And, if background or autofluorescence is involved, the phasors with weak intensities should be moved toward longer lifetime (toward [0,0], lower temperature). However, the phasors with weak intensities are actually at shorter lifetime side (toward [0,1], higher temperature).

Our results suggest that the temperature changes can be tracked at pixel resolution via fluorescence lifetime of RhB in live cells. The parallel multifrequency measurement in one shot allows postanalysis to be done at any allowed harmonic frequency. Furthermore, we can reduce the phase steps from 16 to 8 to increase the speed to ~1 second.

4 | CONCLUSION

We describe testing and applications of a modulated CMOS sensor in widefield FD-FLIM. The flexible coupling and easy setup make it an ideal choice for FLIM applications with any widefield fluorescence microscope, for example, TIRF and SPIM. The pulsed supercontinuum laser and the phasor analysis method further simplified the system construction and data analysis with capability of parallel multifrequency detection. The fast intrinsic response and modulation of this sensor and the 20 MHz picoseconds laser allow a larger number of harmonics to be measured in parallel, that is, from 20 to 620 MHz, which covers most commonly used modulation frequencies in FD-FLIM measurements. In comparison with traditional intensified CCD-based widefield FD-FLIM, this system dramatically reduced complexity of the operation because all the frequency domain operations are embedded in the FPGA of the sensor. Even more, it offers the multifrequency capability with frequency up to 620 MHz, which could not be achieved before. With this system, we analyzed FRET efficiency in cells transfected with a construct of Cerulean-Venus at different frequencies. We were also able to measure the localized temperature change at pixel resolution in HeLa cells via fluorescence lifetime of RhB dye from 22°C to 44°C. In the future, we are expecting to improve the QE of the camera in order to improve the signal level and further improve the imaging speed and reduce laser power, especially in biomedical diagnosis.

ACKNOWLEDGMENTS

This work was supported by the National Institutes of Health NIH P41-GM103540 and NIH P50-GM076516. Also, we would like to thank Milka Stakic for cell culturing.

AUTHOR BIOGRAPHIES

Please see Supporting Information online.

ORCID

Enrico Gratton https://orcid.org/0000-0002-6450-7391

REFERENCES

[1] C. Y. Dong, T. French, P. T. So, C. Buehler, K. M. Berland, E. Gratton, *Methods Cell Biol.* **2003**, *72*, 431.
[2] Y. C. Chen, R. M. Clegg, *Photosynth. Res.* **2009**, *102*(2), 143.
[3] M. Y. Berezin, S. Achilefu, *Chem. Rev.* **2010**, *110*(5), 2641.
[4] E. P. Buurman, R. Sanders, A. Draaijer, H. C. Gerritsen, J. J. F. van Veen, P. M. Houpt, Y. K. Levine, *Scanning* **1992**, *14*(3), 155.
[5] C. G. Morgan, A. C. Mitchell, J. G. Murray, A. C. Michell, *J. Microsc.* **1992**, *165*(1), 49.
[6] D. W. Piston, D. R. Sandison, W. W. Webb, *SPIE* **1992**, *1640*, 379.
[7] P. T. C. So, T. French, W. M. Yu, K. M. Berland, C. Y. Dong, E. Gratton, *Bioimaging* **1995**, *3*(2), 49.
[8] O. Holub, M. J. Seufferheld, C. Gohlke, Govindjee, R. M. Clegg, *Photosynthetica* **2000**, *38*(4), 581.
[9] R. M. Clegg, O. Holub, C. Gohlke, *Methods Enzymol.* **2003**, *360*, 509.
[10] Q. Wu, S. Guo, Y. Ma, F. Gao, C. Yang, M. Yang, X. Yu, X. Zhang, R. A. Rupp, J. Xu, *Opt. Express* **2012**, *20*(2), 960.
[11] H. Chen, E. Gratton, *Microsc. Res. Tech.* **2013**, *76*(3), 282.
[12] J. R. Alcala, E. Gratton, D. M. Jameson, *Instrum. Sci. Technol.* **1985**, *14*(3–4), 225.
[13] E. Gratton, D. M. Jameson, R. D. Hall, *Annu. Rev. Biophys. Bioeng.* **1984**, *13*(1), 105.
[14] E. Gratton, B. Barbieri, *Spectroscopy* **1986**, *1*(6), 28.
[15] A. Squire, P. J. Verveer, P. I. Bastiaens, *J. Microsc.* **2000**, *197*(Pt 2), 136.
[16] A. D. Elder, S. M. Matthews, J. Swartling, K. Yunus, J. H. Frank, C. M. Brennan, A. C. Fisher, C. F. Kaminski, *Opt. Express* **2006**, *14*(12), 5456.
[17] S. Schlachter, a. D. Elder, a. Esposito, G. S. Kaminski, J. H. Frank, L. K. van Geest, C. F. Kaminski, *Opt. Express* **2009**, *17*(3), 1557.
[18] A. D. Elder, C. F. Kaminski, J. H. Frank, *Opt. Express* **2009**, *17*(25), 23181.
[19] J. B. Grimm, B. P. English, J. Chen, J. P. Slaughter, Z. Zhang, A. Revyakin, R. Patel, J. J. Macklin, D. Normanno, R. H. Singer, T. Lionnet, L. D. Lavis, *Nat. Methods* **2015**, *12*(3), 244.
[20] A. Leray, F. B. Riquet, E. Richard, C. Spriet, D. Trinel, L. H. Liot, *Microsc. Res. Tech.* **2009**, *72*(5), 371.
[21] B. A. Feddersen, D. W. Piston, E. Gratton, *Rev. Sci. Instrum.* **1989**, *60*(9), 2929.

[22] M. A. Digman, V. R. Caiolfa, M. Zamai, E. Gratton, *Biophys. J.* **2008**, *94*(2), L14.
[23] A. Esposito, T. Oggier, H. C. Gerritsen, F. Lustenberger, F. S. Wouters, *Opt. Express* **2005**, *13*(24), 9812.
[24] H. Chen, G. Holst, E. Gratton, *Microsc. Res. Tech.* **2015**, *78*(12), 1075.
[25] R. Franke, G. A. Holst, *SPIE BiOS* **2015**, *9328*, 93281K.
[26] J. Bosiers, H. Van Kuijk, W. Klaassens, R. Leenen, W. Hoekstra, W. De Laat, A. Kleimann, I. Peters, J. Nooijen, Q. Zhao, I. T. Young, S. De Jong, K. Jalink, MEM-FLIM, a CCD Imager for Fluorescence Lifetime Imaging Microscopy, in International Image Sensor Workshop, **2013**, 1024, p. 2–5.
[27] Q. Zhao, B. Schelen, R. Schouten, R. van den Oever, R. Leenen, H. van Kuijk, I. M. Peters, F. Polderdijk, J. T. Bosiers, M. Raspe, K. Jalink, J. G. S. de Jong, B. van Geest, K. Stoop, I. T. Young, *J. Biomed. Opt.* **2012**, *17*(12), 126020.
[28] M. Raspe, K. M. Kedziora, B. Van Den Broek, Q. Zhao, S. De Jong, J. Herz, M. Mastop, J. Goedhart, T. W. J. Gadella, I. T. Young, K. Jalink, *Nat. Methods* **2016**, *13*(6), 501.
[29] L. Wei, W. Yan, D. Ho, *Sensors* **2017**, *17*(12), 2800.
[30] M. W. Seo, K. Kagawa, K. Yasutomi, Y. Kawata, N. Teranishi, Z. Li, I. A. Halin, S. Kawahito, *IEEE J. Solid-State Circuits* **2016**, *51*(1), 141.
[31] M. Digman, E. Gratton, *Fluorescence Lifetime Spectroscopy and Imaging*, CRC Press, Boca Raton, Florida **2014**, p. 235.
[32] C. Gosse, C. Bergaud, P. Löw, in *Topics in Applied Physics*, Vol. 118 (Ed: S. Volz), Springer, Berlin Heidelberg **2009**, p. 301.
[33] C. Paviolo, A. H. A. Clayton, S. L. Mcarthur, P. R. Stoddart, *J. Microsc.* **2013**, *250*(3), 179.
[34] D. Moreau, C. Lefort, R. Burke, P. Leveque, R. P. O'Connor, *Biomed. Opt. Express* **2015**, *6*(10), 4105.
[35] R. Mercadé-Prieto, L. Rodriguez-Rivera, X. D. Chen, *Photochem. Photobiol. Sci.* **2017**, *16*(11), 1727.

How to cite this article: Chen H, Ma N, Kagawa K, Kawahito S, Digman M, Gratton E. Widefield multi-frequency fluorescence lifetime imaging using a two-tap complementary metal-oxide semiconductor camera with lateral electric field charge modulators. *J. Biophotonics*. 2019;12:e201800223. https://doi.org/10.1002/jbio.201800223